Summer 2020

Forming and processing of advanced fiber reinforced polymer composites

Robert Meinders

Department: Mechanical and Aerospace Engineering

FORMING AND PROCESSING OF ADVANCED FIBER REINFORCED POLYMER COMPOSITES

by

ROBERT RAYMOND MEINDERS

A DISSERTATION

Presented to the Graduate Faculty of the

MISSOURI UNIVERSITY OF SCIENCE AND TECHNOLOGY

In Partial Fulfillment of the Requirements for the Degree

DOCTOR OF PHILOSOPHY

in

AEROSPACE ENGINEERING

2020

Approved by:

K. Chandrashekhara, Advisor
Ming Leu
V. A. Samaranayake
Thomas Schuman
Xiaodong Yang

PUBLICATION DISSERTATION OPTION

This dissertation consists of the following three articles, formatted in the style used by the Missouri University of Science and Technology:

Paper I, found on pages 3-21, has been published in the proceedings of Composites and Advanced Materials Expo in Anaheim, CA, in September 2019 and is intended for submission to Composites Science and Technology.

Paper II, found on pages 22-39, is intended for submission to Polymer and Polymer Composites.

Paper III, found on pages 40-49, is intended for submission to Journal of Applied Polymer Science.

ABSTRACT

Composite materials are commonly used in industry to manufacture strong and lightweight structures. Composites feature a large degree of flexibility in materials selection and manufacturing processes to tailor the strength of manufactured parts. This study examines different manufacturing aspects of composites. In Part I, the fabrication of composite parts using the compression forming process is examined. During compression forming, metal dies are used to apply large deformations to prepreg material to fabricate composite parts. The high stresses and deformations of this process can yield manufacturing defects. T650/5320-1 prepreg is subjected to material characterization to develop simulations of large deformation forming processes. Material properties pertinent to the deformation process are evaluated using ASTM testing standards. Part II explores transparent composites as a lightweight and tough material that can improve current armor technology. Epoxy resin is formulated to match the refractive index of the fiber reinforcement for the fabrication of transparent composites. Transparent composite panels composed of S-glass fabric and epoxy resin are manufactured using the vacuum-assisted resin transfer molding (VARTM) process to evaluate tension, flexure, and impact resistance properties. Part III investigates renewable resources for polymer composite production. HF-8450 and S300 soybean polyol are studied to produce polymers for continuous fiber-reinforced composites. Formulations of thermoset polyurethane using soy-based polyol are developed for use in composites. Continuous glass fiber-reinforced composite samples are manufactured using the vacuum bagging process and the composite samples are characterized using flexure testing.

ACKNOWLEDGMENTS

I wish to thank Dr. K. Chandrashekhara for guiding me on my journey through higher education. Dr. Chandrashekhara has pushed and encouraged me in my pursuit of knowledge and has shown exceptional patience and expertise to advance my studies.

I would like to thank my committee members Dr. Leu, Dr. Samaranayake, Dr. Schuman, and Dr. Yang for providing encouragement and council during my studies.

I would also like to acknowledge our composite research team: Dr. A. Abutunis, Dr. S. Anandan, Dr. G. Dhaliwal, Dr. M. Fal, Dr. J. Nicholas, Dr. G. Taylor, Mr. S. Dasari, Mr. S. Ganguly, Mr. D. Murphy, Mr. F. Okanmisope, Mr. M. Rangapuram, Mr. D. Ruble, and Mr. A. Wood for providing insight and helpful discussions throughout my research.

I would like to thank the Chancellor's Fellowship for their financial support in my journey through higher education. Without them, I do not think this would have been possible.

I want to recognize Mr. and Mrs. Hester for starting me on my journey in pursuit of a scientific degree. I would like to recognize Mr. D. Cress, Mrs. L. Francis, and Dr. D. Samson for continuing to push me during my time at Missouri S&T. Finally, I would also like to thank my mother, father, sister, and all of my family for believing in me while I reached for the stars.

TABLE OF CONTENTS

Page

LIST OF ILLUSTRATIONS

PAPER I Page

PAPER II

PAPER III

LIST OF TABLES

1. INTRODUCTION

Composites are made up of dissimilar materials to produce new systems with improved properties. A fiber with high stiffness and strength is frequently paired with a lightweight polymer matrix that offers toughness and flexibility to produce materials that can have higher strength to weight ratios than conventional metals. There are a wide range of fibers and polymers used in industry to tailor the material properties of composites to meet the needs of a manufacturer.

1.1. COMPOSITE FORMING

Prepreg materials which consist of fiber reinforcement and uncured resins are used in manufacturing parts because of the ease of use and repeatability. Prepreg materials can be used to make parts in a variety of ways. Compression molding is popular due to its high throughput and repeatability. In compression molding, prepreg materials are joined under high pressures using a closed mold tool to generate parts in the final shape. The forming process generates large displacements within prepreg materials that can produce part defects without careful design. High stresses associated with part formation also contribute to residual stress that can cause finished parts to warp. This encourages iterative designing of the mold tool, but the cost to develop and fabricate molds for this process can hinder its deployment to quickly fabricate parts.

Study of the material reaction forces during compression molding can improve understanding of the forming process and improve the development of new molds for parts. Therefore, the current work provides an experimental outline to evaluate the

properties of prepregs during compression molding and develops simulations to model new tooling for part fabrication.

1.2. TRANSPARENT COMPOSITES

Composites make use of the flexible nature of polymers to provide toughness against impact. By controlling the composition of an epoxy polymer, it is possible to produce a resin system with identical optical properties to the fiber reinforcement in a composite. In particular, matching the refractive indices produces a composite where the fiber reinforcement becomes invisible but still provides strength to the material. In this study, such a transparent composite is produced. The mechanical properties are evaluated for use as a reinforcement to ballistic materials.

1.3. SOY-BASED POLYURETHANES

Polyurethanes are heavily used in manufacturing because of the wide range of material properties that can be developed. Polyurethane can be formulated to produce either thermoplastics or thermosets. Incorporating blowing agents allows for the production of foam materials that can be either rigid or soft.

Polyurethane can be manufactured by the reaction of isocyanate with polyols to generate the polymer chains. Currently, petroleum products are used to manufacture both polyols and isocyanate. The limited nature of petroleum is pushing for renewably sourced polyols and isocyanates. This study examines soy-based polyols for producing polyurethane composites.

PAPER

I. MODELING AND SIMULATION OF POLYMER COMPOSITE PREPREG FORMING PROCESS

Robert Meinders, Shouvik Ganguly, and K. Chandrashekhara

Missouri University of Science and Technology
Department of Mechanical and Aerospace Engineering
Rolla, MO 65409

ABSTRACT

Fabrication of composite materials has been traditionally achieved with the help of metallic molds to ensure proper shape. The development of new forming and molding processes is expensive because the molds to produce parts are made from highly polished metal which can take months to manufacture. These molds need to be tested to ensure high part quality for production. Molds that cannot produce parts to specifications will need to be scrapped and redesigned. Simulation of the mold surfaces and manufacturing process reduces the iterations to produce high quality parts. Forming process for prepreg materials was explored using simulations to study the evolution of defects during the composite forming and layup process. Material characterization of the prepreg materials provides the real properties required for simulation. Shear modulus, stiffness, friction, and peel strength for carbon/epoxy prepreg are determined experimentally for an eight-harness satin weave prepreg. A hemispherical punch and forming die was modeled.

Results are presented for the final shape of the formed part and the nature of forming defects are observed.

1. INTRODUCTION

Significant resources are used each year to decide if a part can be manufactured and to correct manufacturing defects. Numerical and empirical models of composite forming are required to optimize the processing of composite materials prior to tooling fabrication. These forming models require a significant understanding of material characterization and isolation of material properties. There is also a need for numerical modeling techniques that can capture the deformation of the material during composite forming process. A comprehensive numerical and experimental study of composite forming would lead to significant time and cost savings.

Draping and wrinkling are a part of prepreg forming. Simulation of fabric forming process can help to deduce the presence of defects during composite manufacturing. The large deformations and shears that may exist within the forming process affect the part quality. Process simulation allows for prediction of regions of high internal stresses that lead to reduced part strength. This feedback is extremely useful for adapting manufacturing parameters to achieve a better quality product.

Material characterization for forming and layup have been identified as relying on three key mechanisms: a) in-plane mechanisms like fabric shearing, b) inter-ply properties like tack, and c) rate dependent bending and consolidation [1-6]. Each mechanism has various experimental approaches to develop the data. Characterized data

will be reduced into empirical modeling inputs. Abaqus software will be used to develop numerical models of the forming process. Work will be done to characterize and advance the state of the art for modeling composite prepreg forming.

This paper will focus on the development of a simulation for 8-harness weave T650/5320-1 prepreg. Experimental characterization is outlined and performed to generate prepreg properties for simulation. A hemispherical punch and forming die is modeled.

2. EXPERIMENTATION

In order to develop a simulation of the prepreg forming process it is important to determine the reaction forces that the material will generate in response to deformation as well as the material resistance to defects. A series of material characterization experiments were performed to find the material properties of 8-harness T650/5320-1 prepreg material. The material properties were then used to generate forming simulations for the manufacturing process. Material properties required for the simulation are fabric shearing, material tack, material bending, tension, and compression. These properties were obtained through the following experiments.

2.1. BIAS EXTENSION TEST

Bias extension is a variation of tensile testing which measures the in-plane shear response of prepreg materials and the shear locking angle [7-9]. The test uses ±45° prepreg sheets in tension to develop three shear regions: the region adjacent to the clamps

(region C in Figure 1) is not subjected to any shear loading, the central test region (region A in Figure 1) experiences pure shear loading, and the last region (region B in Figure 1) experiences half shear. The reaction forces and shear angles are measured.

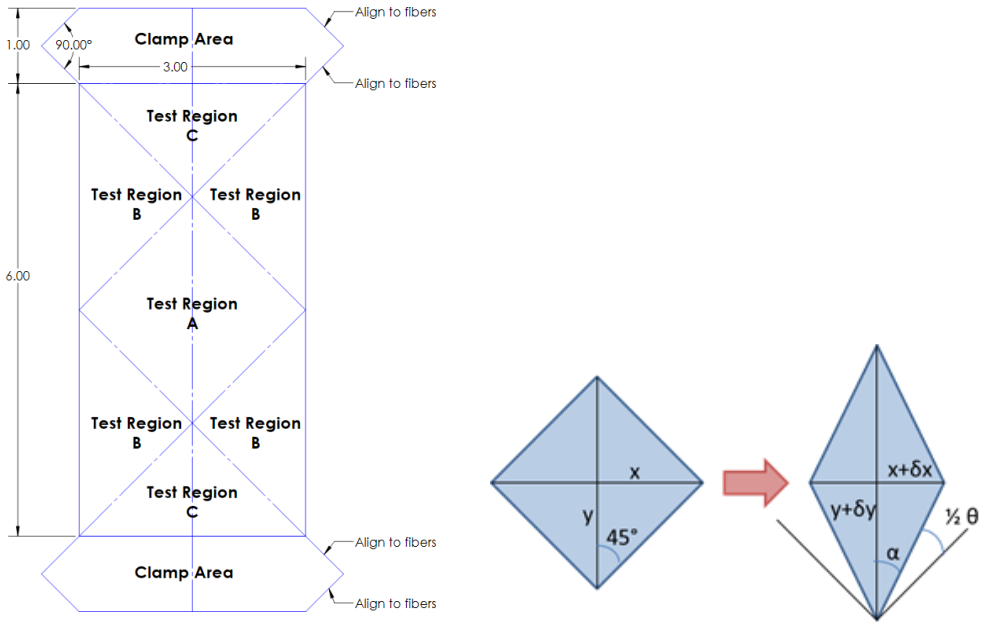

Figure 1. Bias extension test geometry indicating different shear regions (left) and central shear region (right)

The theoretical shear angle θ of the prepreg can be calculated according to Equation 1 based on crosshead displacement for a sample with 2:1 (height to width) geometry.

$$\theta = \frac{\pi}{2} - 2\cos^{-1}\left[\frac{W + D}{\sqrt{2}W}\right] \quad (1)$$

where D is displacement distance and W is sample width.

Visual analysis and measurements are a preferred method to track the shear in the fabric due to the potential for material defects such as fiber pullout and tow slippage.

Samples were visually marked to separate the test regions and the shear angle of region A was measured with a protractor. A video extensometer was also implemented to provide live data acquisition and measure the axial and transverse strains within the pure shear region. Using a video extensometer to measure the longitudinal and transverse strains it is possible to calculate the shear strain.

$$\alpha = \tan^{-1}\left(\frac{x + x\varepsilon_x}{y + y\varepsilon_y}\right) \tag{2a}$$

$$\theta = \frac{\pi}{2} - 2\alpha \tag{2b}$$

where *x* and *y* are the strain gauge lengths and εx and εy are the measured strains. The shear reaction can then be plotted for simulation. In this experiment, samples were cut into 20.3 cm x 7.6 cm (8 in. x 3 in.) sheets with a fiber orientation of 45° to provide a 15.2 cm (6 in.) test gauge length with a 2.5 cm (1 in.) clamp area. The samples were marked for the video extensometer and tested at a constant displacement rate to 2.8 cm (1.1 in.) of displacement to achieve a 60° fiber shear angle.

2.2. T-PEEL TEST

T-Peel test analyzes the out of plane bonding strength of adhesives. It can be used to examine the bond between plies of prepreg and allows for a model of delamination during the forming process to be developed. For this test the ASTM standard D1876 was used as a basis [10].

Two prepreg sheets were cut to 152 mm x 305 mm (6 in. x 12 in.) and bonded together with a light tacking force for 229 mm (9 in.) in the long dimension leaving 76 mm (3 in.) at the end unbonded and separated by a peel film. The tacked sheets were then

cut into identical strips of 25 mm (1 in.) width. The unbonded section of each test strip was then placed into a tensile test fixture on an Instron test frame with a 10 kN load cell and the sample strips were separated at a rate of 254 mm (10 in.)/min and the loads were recorded.

2.3. STIFFNESS TESTING

Stiffness of fabrics can be used to model out of plane reaction forces from fabric bending. The test is based on ASTM D1388 and uses a Taber stiffness tester model 112 for measurements [11]. Fabric bending stiffness can be calculated based on the area density of the material and the length of material overhang required to deflect to a 41.5° angle. Flexural rigidity, *G*, can be calculated in μJ/m using Equation 3.

$$G = 1.421 \times 10^{-5} \times W \times c^3 \tag{3a}$$

$$\text{where, } c = \left(\frac{overhang\ length}{2}\right) \tag{3b}$$

where *c* is expressed in mm and *W* is the density of the fabric in g/m^2.

Strips of prepreg measuring 203.2 mm x 25.4 mm (8 in. x 1 in.) were cut and allowed to reach ambient temperature. Samples were measured and weighed to find the areal density of the prepreg. Samples were then placed on a leveled test bed and the test sled slowly extended until the prescribed deflection was reached.

2.4. NUMERICAL HOMOGENIZATION

Numerical homogenization is a process used to determine the effective material properties of a composite material. These material properties are used as inputs to represent the composite in simulation [12, 13]. The effective properties of a unit cell

structure can be determined from the elastic stress strain constitutive relation. Plane stress is assumed in this case because of the small thickness compared to the unit cell width and length. Periodic boundary conditions are applied to the unit cell by constraining the representative volume element so that only one dimension of strain exists at a time. The effective stress strain relation is provided in Equation 4.

$$\begin{Bmatrix}\sigma_{11}\\ \sigma_{22}\\ \sigma_{12}\end{Bmatrix} = \begin{bmatrix}C_{11} & C_{12} & 0\\ C_{12} & C_{22} & 0\\ 0 & 0 & C_{66}\end{bmatrix}\begin{Bmatrix}\varepsilon_{11}\\ \varepsilon_{22}\\ \varepsilon_{12}\end{Bmatrix} \tag{4}$$

Applying only one strain in a simulation allows for an estimate of the respective stiffness coefficient of the material. By simulating a single strain in each principal direction the material stiffness in the principal directions can be estimated. In this way the stiffness matrix and effective material properties can be evaluated for the bulk. Numerical homogenization was used to evaluate the material properties of the prepreg in tension and compression. This allows for an estimate of the material reaction in compressive loading where tests would not be possible.

3. RESULTS

3.1. BIAS EXTENSION TESTING ANALYSIS

The test was performed on six sets consisting of five samples at different crosshead displacement rates: 0.254 mm/s, 1.27 mm/s, 2.54 mm/s, 5.08 mm/s, 7.62 mm/s, and 10.16 mm/s (0.01 in/s, 0.05 in/s, 0.1 in/s, 0.2 in/s, 0.3 in/s, and 0.4 in/s). An Instron 5985 frame with 10kN load cell and custom clamping fixture were used for the test. Samples were marked to allow visual analysis by tracing the fibers that represent the edge

of the shear regions. Shear angles of the specimens were tracked using an Instron video extensometer set to measure both longitudinal and transverse strains in the pure shear region (Figure 2).

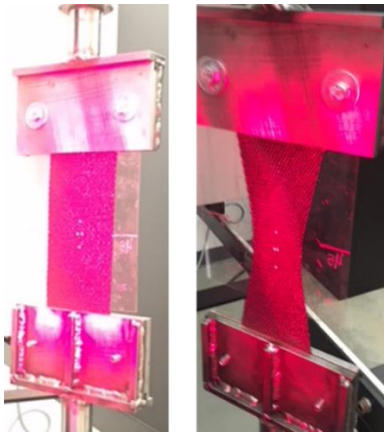

Figure 2. Bias extension test (pre and post extension)

The reaction forces generated within the prepreg were very low at small shear angles as the slack between fibers was removed. The fabric exhibited a large region of nearly linearly increasing shear force as the shear angle rose. For the 8-harness weave the locking angle appears to exist around 33° of shear. Afterwards the load increases rapidly as fiber locking mechanisms resist further extension. The force results for the different testing rates can be seen in Figure 3 and are summarized in Figure 4.

From the test it was apparent that the shearing forces are highly dependent on shearing rates. The tests also indicated the presence of viscous forces as the measured loads would relax at the end of the test without reducing the amount of shear.

Disagreement between theoretical shear angle and measured shear angle was observed during the bias extension test (Figure 5). This is indicative of fiber tow slipping

and irreversible losses from the prepreg fabric during the test and matches the results of Harrison [9].

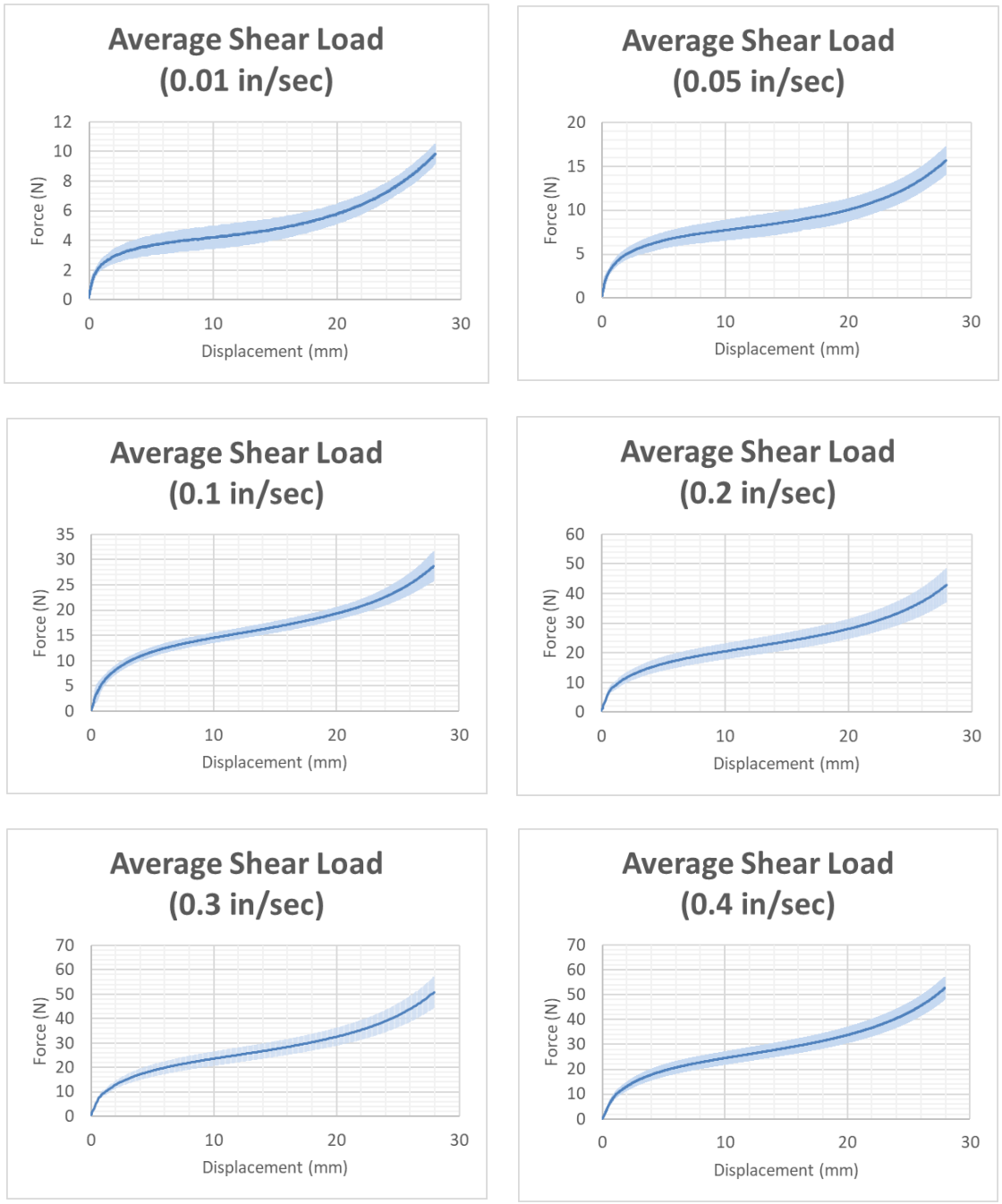

Figure 3. Force vs displacement in bias extension test at different strain rates. Average Force-blue; Standard Deviation-shaded regions

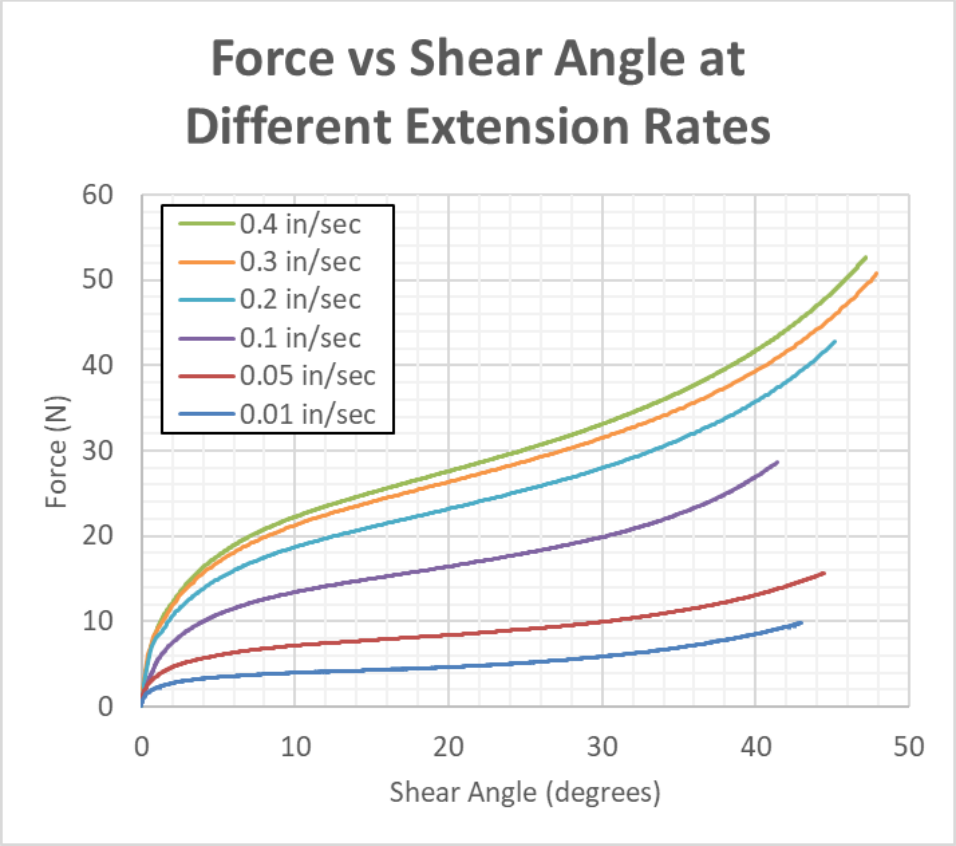

Figure 4. Reaction force vs measured shear angle

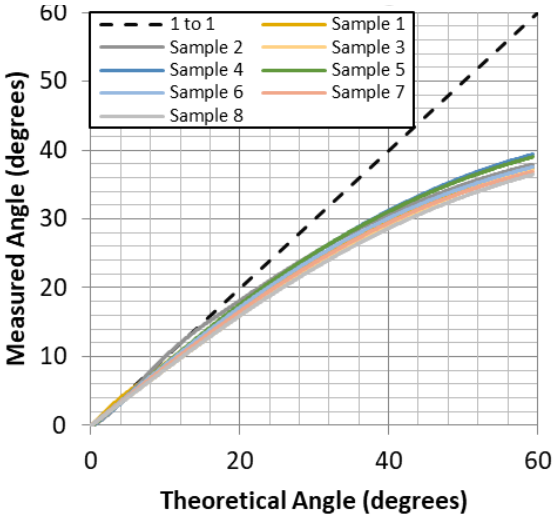

Figure 5. Comparison between ideal shear case and measured shear angles

3.2. T-PEEL TEST RESULTS

T-peel test of the prepreg was performed using ASTM D1876 as a basis. Five samples were prepared at ambient conditions and lightly pressed together to estimate the epoxy adhesion between adjacent plies. Samples were tested on an Instron 5985 test frame with a 10 kN load cell using tensile grips. Forces were recorded and normalized to the width of the specimens. The tested samples exhibited elastic response until peeling between plies initiated. There was a small decrease in load and the load remained steady over a 127 mm region of separation. The peak load for peel initiation and average peeling load is reported in Table 1.

Table 1. T-Peel test results for prepreg

	Maximum Load (N/mm)	**Average Peel Load (N/mm)**
Average	0.853	0.543
Standard Deviation	0.138	0.103

3.3. TABER STIFFNESS TEST

Fabric stiffness testing was performed using ASTM D1388 and a Model 112 Taber Stiffness Tester. Eight samples of prepreg were tested. The samples were weighed on a digital scale to find the area density of the prepreg. The tester was leveled and clamped to a table. The prepreg samples were loaded onto the tester and a slow cranking action was used to drive the sled forward for the test. Test results are reported in Table 2.

Table 2. Taber stiffness results

Property	Average	Standard Deviation
Density (g/m^2)	588	10.3
Overhang Length (mm)	107	2.14
Bending Length (mm)	53.6	1.07
Flexural Rigidity (μJ/m)	1292	93.9

3.4. NUMERICAL HOMOGENIZATION

Unit cell modeling was performed to determine the axial material response to tension and compression for modeling. Material properties for the T650 fabric and Cycom 5320-1 resin were taken from literature and applied to Abaqus simulations [14-16]. Fibers and matrix 3D meshes were generated using Texgen freeware. Based on our initial results, it was apparent that a full eight fiber weave was computationally expensive to evaluate and a reduced problem was proposed and simulated. Two sub sets of fiber meshes were simulated, the double over and the single weave pattern (Figure 6), to generate properties for the fiber geometry within the 8-harness weave pattern. The material properties for each subset were determined for the longitudinal and transverse directions for tension and compression. The material properties were then assigned within a larger part while assuming plane stress condition and using shell elements (Figures 7 and 8).

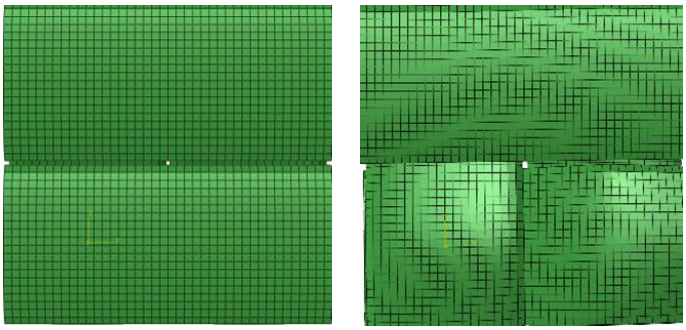

Figure 6. The “double over” (A) and “single weave” (B) fiber meshes

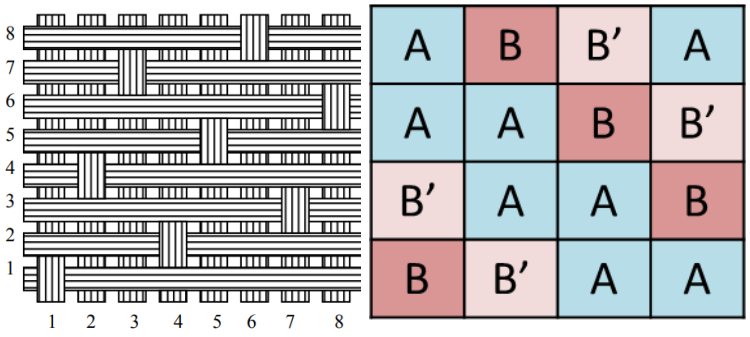

Figure 7. Sample of 8-harness weave and quilt block pattern

Figure 8 depicts the simulation of the full 8-harness fabric after applying the material properties of the two sub sets of fiber meshes. The fabric was constrained in the same fashion as previously described to allow for the axial stiffness to be calculated for both the x and y direction. The drastic changes in material properties between the A and B unit cells led to stress concentrations and discontinuities within the fabric as can be seen by the increase of in-plane principal stress as seen in Figure 8.

The 8-harness fabric was simulated in tension and compression in both the longitudinal and transverse directions. Using numerical homogenization, it was possible to estimate the tensile and compressive stiffness of the prepreg material varying with

strain. The bulk stiffness properties obtained (Figure 9) were utilized for simulating the prepreg during forming.

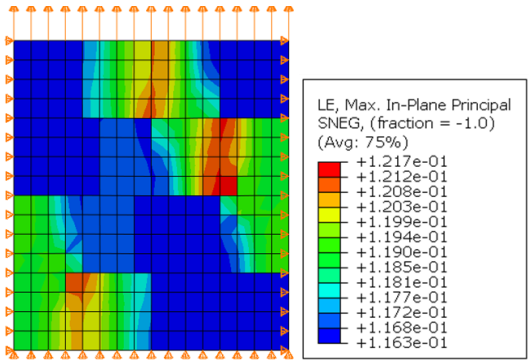

Figure 8. Numerical homogenization of prepreg (total in plane principal strain)

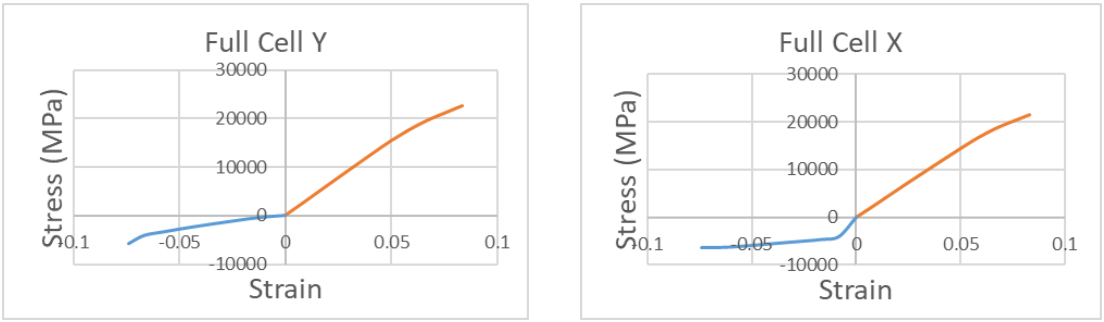

Figure 9. Homogenized stress and strain relations for 8-harness prepreg

3.5. FORMING SIMULATION

Simulation of a 0.1 m radius hemispherical punch was performed in Abaqus using the Fabric user subroutine. A flat tool plate 1 m x 1 m with 0.101 m radius hole served as the resting surface. The tooling components were modeled as 3D discrete rigid. Fabric was modeled as 3D deformable shell. The fabric was constrained in out of plane direction

along its edges. The stiffness for the material obtained by using numerical homogenization was used for forming simulations.

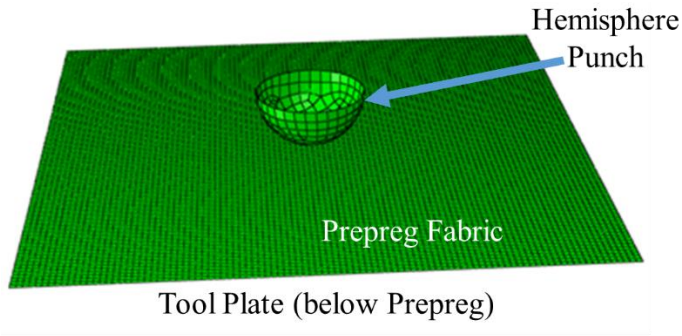

Figure 10. Fabric forming model geometry showing punch and fabric initial position

During simulation the punch was moved by a set displacement to provide the forming mechanism within the simulation. Forming analysis on a single ply model showed the formation of high strain regions along the 45° orientations at the edge of the tool punch.

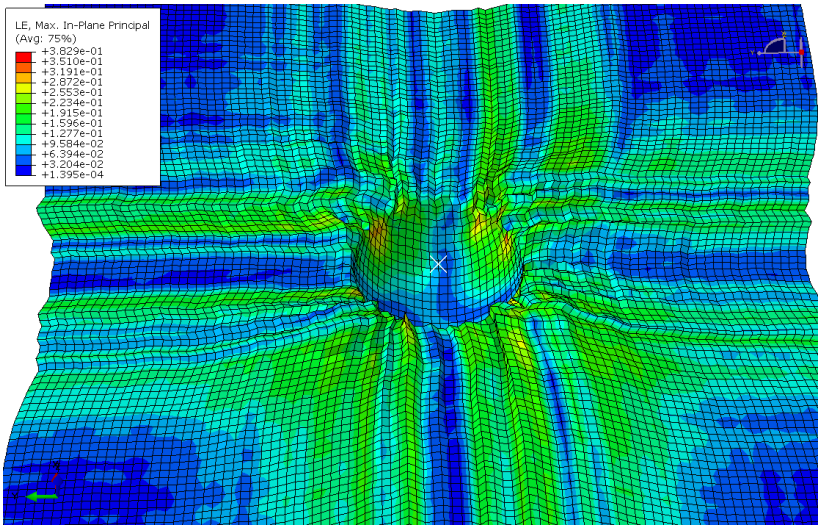

Figure 11. Simulation of fabric forming process for 8-harness prepreg

From this simulation it would be suggested that additional tension forces would be applied through the laminate to reduce the amount of out of plane deformations and to reduce the possibility of buckling.

4. CONCLUSIONS

Material characterization of uncured prepregs is currently underutilized. Defining the material properties and responses during the layup and forming process will help improve process performance and reduce defects and other manufacturing errors. Material characterization will also help to evaluate ideas for new parts and check for high repeatability by reducing regions of high forming stresses and zones with elevated likelihood of wrinkles. The forming process can be used to produce parts that involve high shear displacements. Simulation of the forming process can identify forming geometries where undesirable defects such as wrinkling or fiber misalignment may occur. Simulation can help to find solutions to these defects in the form of increasing fabric tension or altering the deformation rates. The implementation of simulation can also reduce the cost of development to manufacture new parts by identifying tooling that will not produce satisfactory components and allow for design changes before tooling is manufactured.

This study has focused on the material characterization required to generate simulations of the prepreg forming process. Material properties such as in-plane shear, fabric stiffness, and prepreg tack were experimentally measured for an 8-harness prepreg. Simulations of the material were used to determine the prepreg reaction to compressive

loading. Forming simulations of the prepreg were also performed to evaluate the feasibility of the simulation and check the proposed tooling for regions of wrinkling and defect formation. The current study was limited to thin prepreg forming simulations using fabric models to predict the possibility of wrinkling. Future work will focus on simulating thicker laminate interactions and stacking effects within manufactured parts. A forming experiment to evaluate the simulation results will also be performed.

5. ACKNOWLEDGEMENT

The authors would like to acknowledge the support from the Center for Aerospace Manufacturing Technologies (CAMT). The authors would like to thank Dr. Tim Luchini (Boeing) for his helpful suggestions.

REFERENCES

1. Wang, J. “Predictive Modelling and Experimental Measurement of Composite Forming Behaviour.” (PhD Thesis) *The University of Nottingham*, 2008.

2. Farnand, K.A. “Process-Induced Wrinkling and Waviness in Prepreg Charge-Forming.” (Master’s Thesis) *The University of British Columbia,* 2016.

3. Lightfoot, J.S., Wisnom, M.R., and Potter, K. "A New Mechanism for the Formation of Ply Wrinkles Due to Shear between Plies." *Composites Part A: Applied Science and Manufacturing* Vol. 49, pp. 139-147, 2013.

4. Boisse, P., Hamila, N., Vidal-Salle, E., and Dumont, F. “Simulation of Wrinkling During Textile Composite Reinforcement Forming. Influence of Tensile, In-plane Shear and Bending Stiffnesses.” *Composites Science and Technology,* Vol. 71, pp. 683-692, 2011.

5. Larberg, Y. “Forming of Stacked Unidirectional Prepreg Materials.” (Doctoral Thesis) *KTH Engineering Sciences*, 2012.

6. Bussetta, P., and Correia, N. “Numerical Forming of Continuous Fibre Reinforced Composite Material: A Review.” *Composites Part A*, Vol. 113 pp. 12-31, 2018.

7. ASTM International. *D8067/D8067M-17 Standard Test Method for In-Plane Shear Properties of Sandwich Panels Using a Picture Frame Fixture*. West Conshohocken, PA, 2017. Web. 31 Jan 2018. <https://doi-org.libproxy.mst.edu/10.1520/D8067_D8067M-17>

8. Peng, X., and Cao, J. “Bias Extension Test Standard.” handout. Northwestern University. Evanston, IL. August 2003.

9. Harrison, P., Clifford, M.J., Long, A.C. “Shear characterisation of viscous woven textile composites: a comparison between picture frame and bias extension experiments.” *Composites Science and Technology*, Vol. 64 pp. 1453-1465, 2004.

10. ASTM International. *D1876-08(2015) e1 Standard Test Method for Peel Resistance of Adhesives (T-Peel Test)*. West Conshohocken, PA, 2015. Web. 31 Jan 2018. <https://doi-org.libproxy.mst.edu/10.1520/D1876-08R15E01>

11. ASTM International. *D1388-14e1 Standard Test Method for Stiffness of Fabrics*. West Conshohocken, PA, 2014. Web. 28 Feb 2018. <https://doi.org/10.1520/D1388-14E01>

12. Bheemreddy, V., Chandrashekhara, K., Dharani, L.R., and Hilmas, G.E., “Computational Study of Micromechanical Damage Behavior in Continuous Fiber-reinforced Ceramic Composites,” *Journal of Materials Science*, Vol. 51, pp. 8610 - 8624, 2016.

13. Hussein, R., Anandan, S., and Chandrashekhara, K. "Anisotropic Oxidation Prediction Using Optimized Weight Loss Behavior of Bismaleimide Composites." *Journal of Materials Science*, Vol. 51, no. 15, pp. 7236-7253, 2016.

14. Cytec Industries. “CYCOM 5320-1 Epoxy Resin System.” Booklet. Cytec Industries Inc. October 2015.

15. Cytec. *Thornel T-650/35 PAN-Based Fiber. Thornel T-650/35 PAN-Based Fiber*, 2012.

16. Man, Michelle. *Solvay Cytec Cycom 5320-1 T650 Unitape Qualification Material Property Data Report*.

II. DEVELOPMENT OF FIBER REINFORCED TRANSPARENT COMPOSITES

Robert Meinders, David Murphy, Gregory Taylor, Thomas Schuman, and K. Chandrashekhara

Missouri University of Science and Technology
Department of Mechanical and Aerospace Engineering
Rolla, MO 65409

ABSTRACT

In this study, a continuous glass fiber-reinforced composite is manufactured using the vacuum assisted resin transfer molding (VARTM) process. The composite is manufactured from an S-glass fiber acting as reinforcement and an epoxy resin as matrix. Unlike a traditional E-glass fiber reinforcement, S-glass fibers give higher stiffness and provide easier manufacturability due to the value of the refractive index of S-glass lying within the range of refractive indices of the epoxy resin. The epoxy resin is synthesized Epon 826, Epalloy 5200, and Hexahydropthalic anhydride and tailored to match refractive indices of the S-glass fibers. After synthesis of the resin, composite panels are manufactured from the synthesized epoxy resin and S-glass fibers with a bi-directional 0°/90° 8-Harness satin weave. VARTM process was utilized to manufacture the composite panels. Composite panels are visually inspected for transparency, and tensile, flexural, and impact testing is performed. Mechanical tests showed consistent results for tensile modulus, tensile strength, flexural modulus, flexural strength, and impact damage resistance.

1. INTRODUCTION

The most common transparent material utilized today is glass. While glass can be used for its hardness, strength, chemical resistance, and abrasion resistance, its primary disadvantages are the catastrophic or brittle nature exhibited upon failure and the weight of a pure glass material. Composites offer a lighter and often stronger alternative to glass and similar materials for applications in which weight of material can greatly impact the performance of a structure. However, composites are traditionally heterogeneous, and therefore are difficult to make transparent. The idea of manufacturing a transparent composite relies heavily on matching and maintaining the refractive index match between both the fiber and the matrix [1, 2]. The applications of an optically clear composite include ballistic armor, strengthened windows for vehicles, aircraft, or buildings, and visors for eyewear [3, 4].

Recently researches have approached transparent composites in several different ways, but the main driving force for successful manufacturing of a transparent composite is for armor applications. Strassburger et. al [5] studied projectile impact on several types of transparent armor materials currently in use. Sun et. al [6] modeled different projectile impacts on various transparent armor systems. While maintaining the goal of transparent armor, several researchers have been investigating thermoplastic polymers rather than thermoset polymers. Stenzler and Goulbourne [7] investigated the impact properties of PMMA and PC multilayered composite laminates. A more common topic in transparent composites is transparent nanocomposites. Nanocomposites benefit from increased transparency when compared to short fiber or continuous fiber composites. Retegi et. al

[8] created an all-renewable resource transparent nanocomposite using epoxidized soybean oil and bacterial cellulose nanofibers. Rai and Singh [9] combined both thermoplastic and nanocomposite materials through the manufacture and evaluation of the impact behavior of the composite panels.

However, the ideal goal of transparent composite is to manufacture a continuous fiber composite to maximize the possible structural properties. Krug et. al [10] manufactured a high-performance composite using a UV cure for an epoxy-resin system and S-glass fibers. Results showed high strength due to the S-glass, but transparency became an issue with yellow and blue dispersion occurring on final samples. M. Velez et. al manufactured transparent panels as well but utilized a special rectangular cross-section fiber to reduce dispersion in the composite panels. Additionally, a finite element model was developed to study the impact behavior of the transparent panels.

In the current study, a continuous fiber-reinforced transparent composite is manufactured from S-glass woven fibers and a specially tailored resin with a matching refractive index. The S-glass woven fabric is selected due to the high strength of fibers, high impact resistance of the weave, and better refractive index matching with the epoxy resin system. The resin system is composed of several commercially available epoxies that cure to match the refractive index of the fibers. Composite panels are manufactured with VARTM, and the panels are tested for both tensile and flexural properties following ASTM standards.

2. MATERIALS

2.1. FIBER REINFORCEMENT SELECTION

An S-glass woven fabric manufactured by BGF Industries is used as the fiber reinforcement in the transparent composites. The reinforcement consists of a bi-directional 0°/90° 8-Harness Satin weave. The fabric has a weight of 303.5 g/m² (8.95 oz/yd²) and thickness of 0.23 mm (0.009) in. The refractive index of the fibers is reported by BGF Industries to be approximately 1.522 (Table 1).

Table 1. Refractive indices of fiber and resin

Materials	**Manufacturer**	**Refractive Index**
Epon 826	Momentive	1.573
Epalloy 5200	Emerald	1.486
HHPA	Dixie	1.47
S-Glass	Owens Corning	1.522

2.2. EPOXY SELECTION AND SYNTHESIS

To synthesize a compatible resin with a matching refractive index equal to the fiber refractive index, a resin system needs to consist of at least two parts to tailor a refractive index based on the volume of each of the constituents. In order to maintain a stoichiometric balance between both epoxy and cure hardener, a second epoxy is introduced. The two epoxies chosen for the resin system are Epon 826 from Momentive Performance Materials and Epalloy 5200 from Emerald Performance Materials. The cure

hardener selected for the resin system is Hexahydrophthalic anhydride (HHPA) from Dixie Chemical. The refractive index of the liquid epoxies and cure hardener are shown in Table 1. A transparent catalyst is also utilized to initiate the chain growth but is ignored in regards to the refractive index due the minimal amount of catalyst needed compared to other constituents.

The synthesis of the resin consisted of varying the amount of the two epoxies to modify the refractive index of the resulting resin. All samples were composed of a constant amount of HHPA and catalyst. The HHPA was held constant according to a 1:1 stoichiometric balance between total epoxy and cure hardener. The total amount of epoxy was varied between 100% Epon 826 and 100% Epalloy 5200. Resins were manufactured with these epoxy ratios and narrowed incrementally until a refractive index was matched with the S-glass fibers. The refractive index is matched to the S-glass fibers by curing a small amount of a resin formulation and S-glass fibers in aluminum pans. The cure cycle of the resin system is a 110°C cure for one hour and is further discussed in Section 3. Upon curing, the aluminum pans are peeled, and the resulting sample (Figure 1) is visually inspected for a matching refractive index. The resulting resin system is shown in Table 2.

3. MANUFACTURING

To manufacture the transparent composites from the S-glass fibers and epoxy resin system, the vacuum assisted resin transfer molding process (VARTM) was selected due to the ease of manufacture of the composite panels. The process is similar to a typical

Table 2. Resin system

Material	**Refractive Index**	**Mass (g)**
Epon 826	1.573	13.929
Epalloy 5200	1.486	38.646
HHPA	1.47	46.928
Catalyst	Unknown	0.497
Resin Total	~1.522 (cured)	100

Figure 1. Resin sample matching test with S-glass fibers

autoclave process in which the composite is manufactured under a sealed vacuum bag for the given cure cycle. The major difference of the two processes is lack of a pressurized atmosphere for the VARTM process. The VARTM process operates entirely at atmospheric pressure (101 kPa).

The manufacture of the transparent composites utilizes a two-part mold consisting of a large glass mirror (60 cm x 60 cm) for the base support and a small glass square (18 cm x 18 cm x 0.64 cm) for the upper mold. The glass mirror and glass square are selected due to their polished surface finish. The transparency of a panel is greatly influenced by the surface quality, and therefore, molds with a polished surface provide the best opportunity for composite transparency. Before manufacturing, the surfaces of both molds are cleaned and prepared with the application of a two-part release agent. The release agent consists of Chemlease 15 Sealer EZ and Chemlease® PMR-90 EZ from Chem Trend.

After preparation of the molds, four layers of the S-glass woven fabric are laid up in between the two molds as shown in Figure 2. Sealant tapes are positioned around the edges of the glass mirror mold and vacuum tube inlet and outlet are position on either side of the fiber layup. The glass square mold is placed directly on the fibers, and the glass mirror mold is prepared for infusion (Figure 3). A vacuum bag is applied, and a vacuum is connected to the layup before the infusion to check for any leaks in the layup.

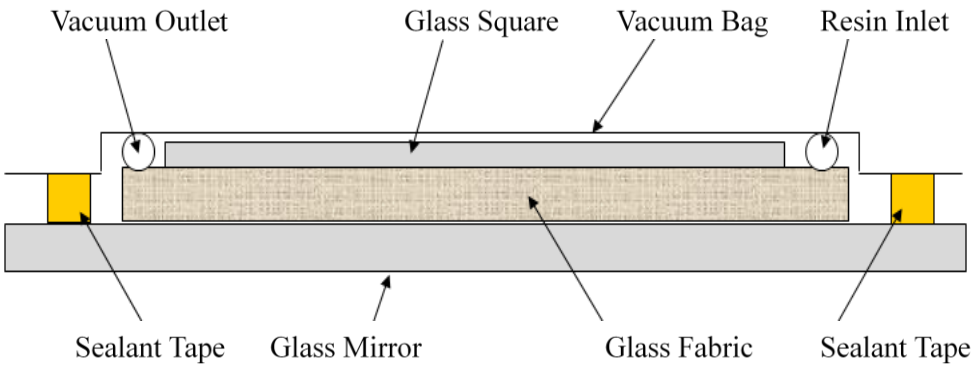

Figure 2. VARTM process schematic for transparent composites

The infusion process for VARTM consists of applying a vacuum to the mold and heating both the layup and epoxy resin to 50˚C. Once the resin system has fully reached 50˚C, the inlet line is opened to allow the epoxy resin to flow into the layup. Throughout the entirety of the infusion, both the layup and resin are maintained at 50˚C to keep a low resin viscosity. With the resin open to the atmosphere, the resin is pushed through the layup which is under vacuum. The resin flows from the inlet into the fibers and across the mold towards the outlet. Once the resin has fully infused the part, the inlet and outlet are sealed to prevent any air from entering the layup. The layup is then placed under the resin cure cycle of 110˚C for one hour (Figure 4). After curing, the transparent panel is examined for visible voids, microscopic voids, surface finish, and refractive index matching. If the sample contained few or no visible (non-microscopic) voids, the sample was cut and prepared for additional testing.

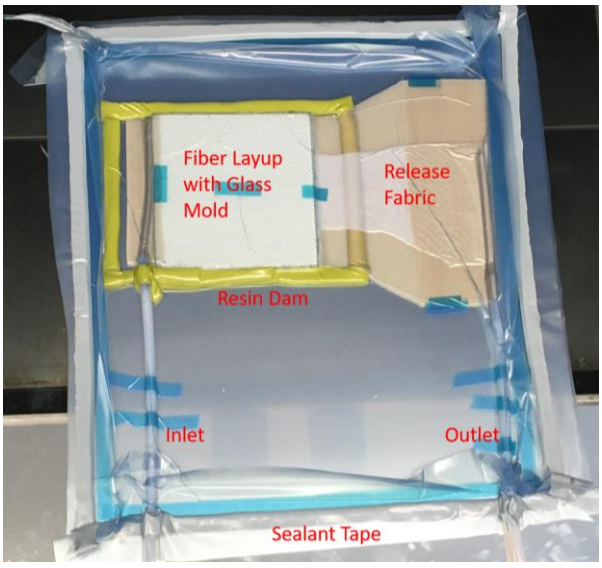

Figure 3. VARTM layup for infusion

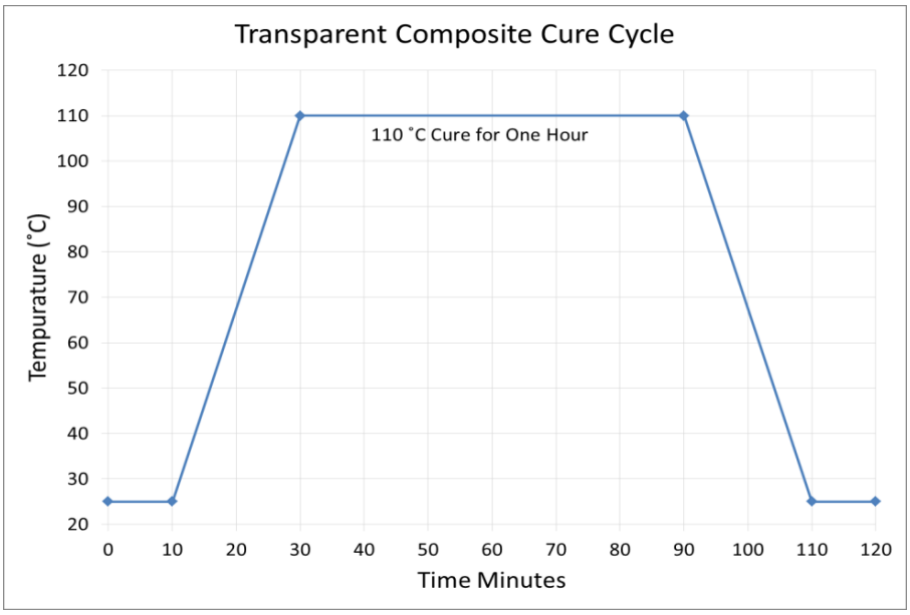

Figure 4. Transparent composite cure cycle

4. EXPERIMENTAL METHODOLOGY

4.1. TENSION TEST SPECIFICATIONS

All tension tests were conducted according to ASTM D3039– 17 Standard Test Method for Tensile Properties of Polymer Matrix Composite Materials [12]. Five samples are cut to approximate dimensions of 152.4 mm x 12.7 mm x 1.14 mm (6 in. x 0.5 in. x 0.045 in.). Precise dimensions for each sample are recorded before each test. For the video extensometer, the gauge length is marked as two black dots approximately 1 in. apart on all samples (Figure 5). The tensions tests are conducted on an Instron 5985 universal testing machine. Load and deflection are recorded along with strain from the video extensometer. Stress is determined after testing from load and sample dimensions.

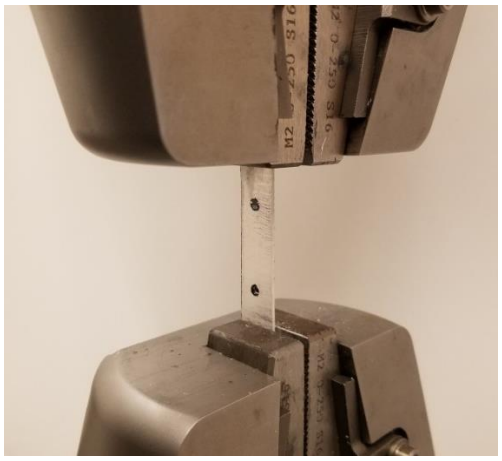

Figure 5. Tension test setup for transparent composites

4.2. FLEXURE TEST SPECIFICATION

All flexure tests were conducted according to ASTM D7264–15 Standard Test Method for Flexural Properties of Polymer Matrix Composite Materials [13]. The four-point bend test is used due to heterogeneous materials composing the composite. Four samples are cut to dimensions of 152.4 mm x 12.7 mm x 1.52 mm (6 in. x 0.5 in. x 0.06 in.). In accordance with ASTM D7264, samples are chosen to be tested with a 60:1 span-to-thickness ratio due to the thickness of the transparent panels, and each have a span of 91.44 mm (3.6 in.). The test speed is 1 mm/min calculated as

$$R = \frac{ZL^2}{6d} \tag{1}$$

where R is test speed in mm/min, Z is rate of straining of the outer fiber (provided as 0.01 mm/mm/min), L is the span in mm, and d is the width of the beam in mm. The test setup is shown in Figure 6.

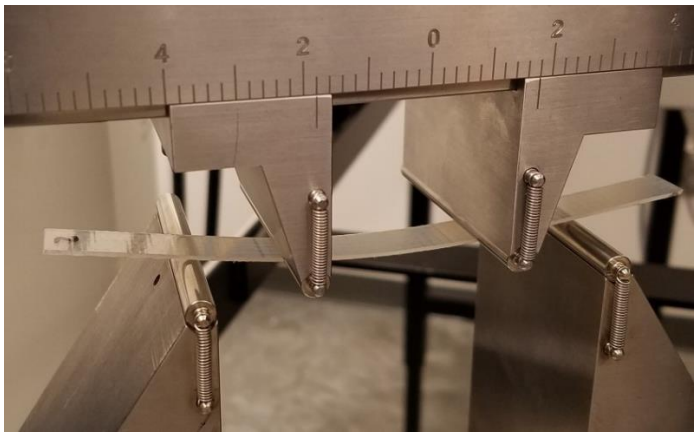

Figure 6. Four-point flexure test setup for transparent composites

4.3. IMPACT TEST SPECIFICATIONS

All impact tests were performed using ASTM D7136/D7136M-15 Standard Test Method for Measuring the Damage Resistance of a Fiber-Reinforced Polymer Matrix Composite to a Drop-Weight Impact Event [14]. Impact testing was conducted on an Instron Dynatup 9250 HV frame. The samples were impacted by a 6.435 kg drop weight with a 12.7 mm diameter impactor pin with a rounded tip. The drop height was adjusted to generate 2 and 5 J/mm impact forces. Samples were held during the impact tests by two clamping plates.

5. RESULTS

5.1. TENSION TEST RESULTS

All five tension samples were successfully tested. Of the five samples, four broke within the gauge section, and the fifth sample's tensile modulus and strength were within the standard deviation of the other four samples. The tensile samples had a tensile

modulus of 17.86 ± 1.32 GPa and tensile strength of 624.6 ± 32.8 MPa. The tensile stress-strain curves for the transparent composite samples are shown in Figure 7.

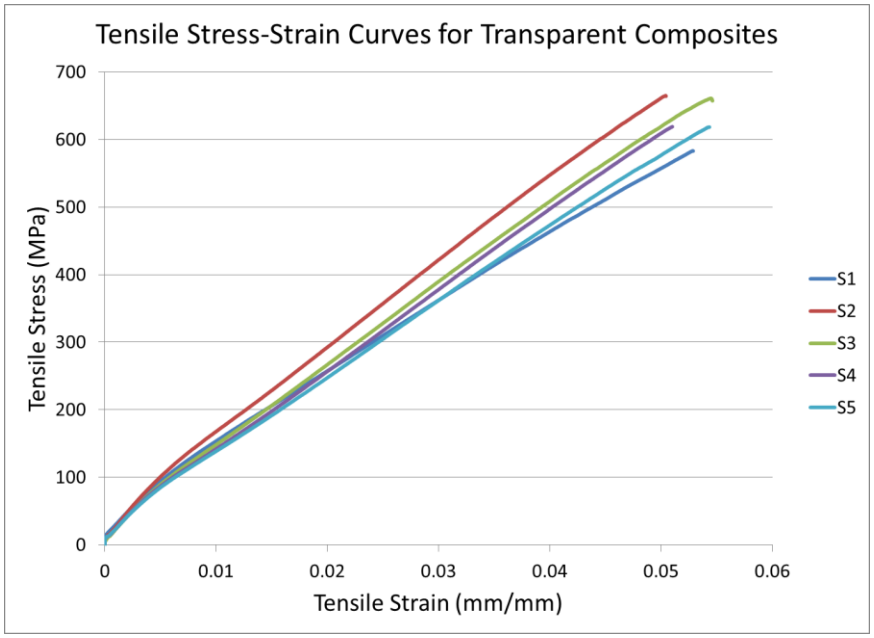

Figure 7. Tensile stress-strain curves for the transparent composite

5.2. FLEXURE TEST RESULTS

All four flexure samples were successfully tested. The four samples did not fail, but the tests stopped due to the stagnation of the flexure stress with increasing strain. The flexural samples had a flexural modulus of 19.69 ± 1.23 GPa and flexural strength of 155.7 ± 3.8 MPa. The flexural stress-strain curves for the transparent composite samples are shown in Figure 8. Due to a low load (40 N) on a 10 kN load cell, the samples displayed some fluctuation in the values of flexural stress near the yield point. However, the results show a consistent value for both flexural modulus and strength.

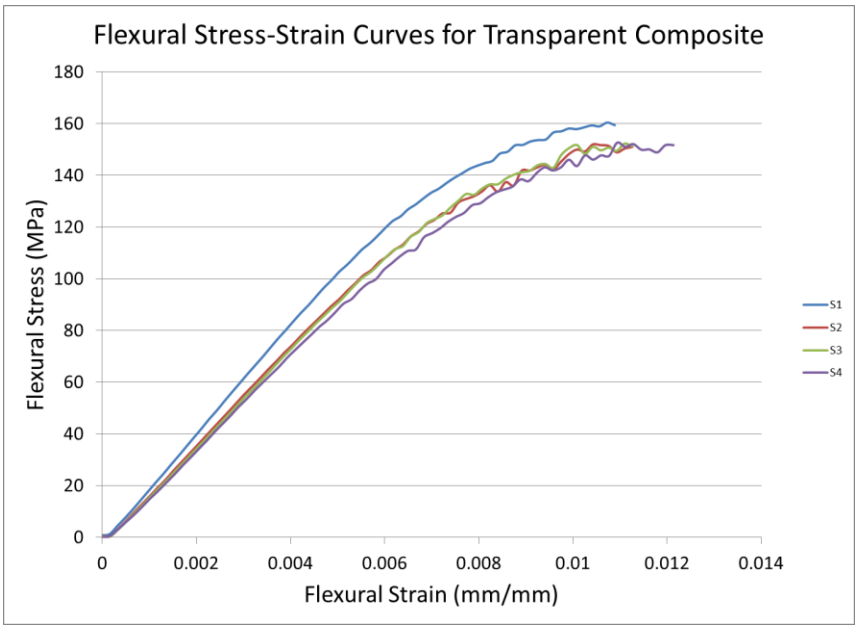

Figure 8. Flexural stress-strain curves for the transparent composite

5.3. IMPACT TEST RESULTS

Two identical plates (A and B) were prepared to supply six samples per energy level. Sample were hit with a nominal 2 and 5 J of energy and the reactions were recorded. The low energy impact had a peak load of 1.325 ± 0.103 kN. This generated an impact energy of 2.383 ± 0.018 J. The low enrgy impact produced some visible internal delaminations within the transparent plate (Figure 9 on left). The transparent composites absorbed 0.919 ± 0.341 J of energy (Figure 10). The results are compiled in Table 3.

The high energy impact had a peak load of 2.084 ± 0.293 kN. This produced an impact enrgy of 5.639 ± 0.046 J. The high energy impact produced visible internal delaminations and cracks accompanied by some fiber breakage which was particularly evident within the B samples (Figure 9 on right). The average absorbed energy was 3.515 ± 1.081 J (Figure 11). The results are compiled in Table 4.

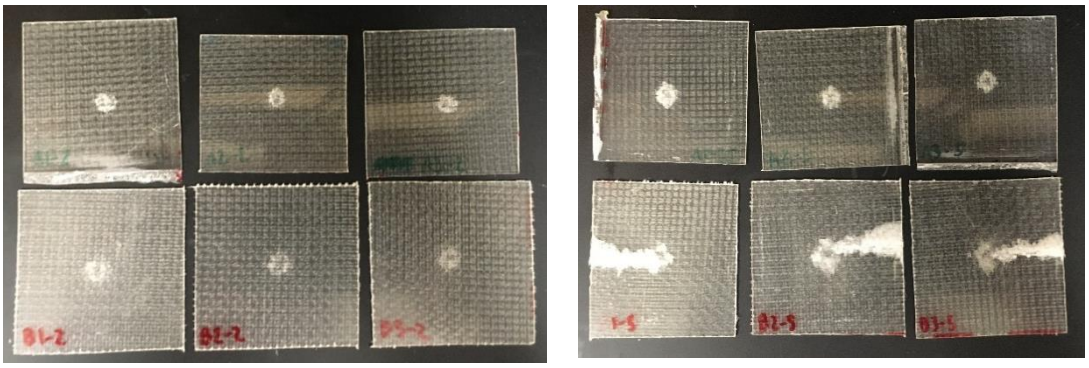

Figure 9. Samples after impact (2J left, 5J right; A top, B bottom)

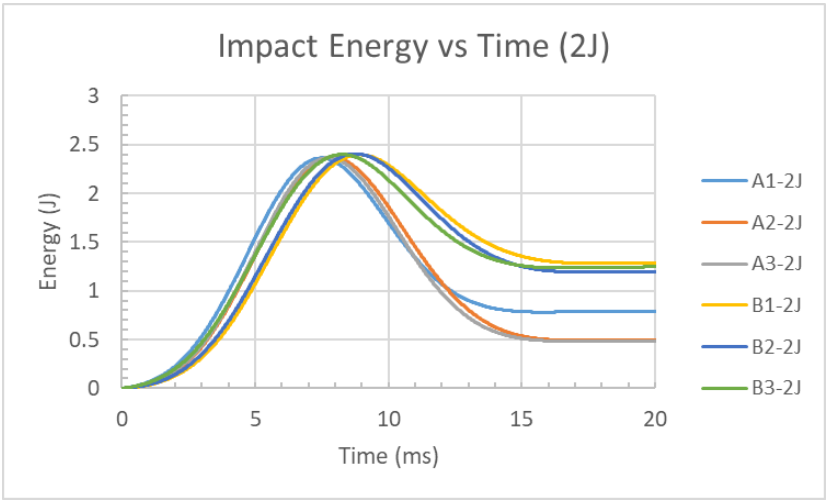

Figure 10. Energy vs time for 2J impact of transparent composites

6. CONCLUSIONS

An epoxy resin system was synthesized from epoxy systems Epon 826 and Epalloy 5200, and cure hardener HHPA. The resin system was tailored to match the refractive index of an S-glass woven fabric upon cure. VARTM layup was used to produce transparent composite panels by infusing the epoxy resin into an S-glass continuous fiber mat. The VARTM layups were then cured at 110 ºC for one hour.

Samples were examined for visual transparency upon curing. The panels were tested for tensile, flexural, and impact properties. The resulting tensile modulus was

Table 3. Impact results for 2J impact test on transparent composite

Sample	**Thickness (mm)**	**Max Force (kN)**	**Peak Energy (J)**	**Absorbed Energy (J)**	**Resting Energy (J)**	**Damage Area (mm^2)**
A1-2J	1.016	1.437	2.362	0.796	1.566	38.601
A2-2J	1.041	1.399	2.367	0.498	1.868	27.217
A3-2J	1.041	1.443	2.366	0.488	1.877	32.389
B1-2J	0.991	1.210	2.397	1.285	1.112	41.043
B2-2J	0.965	1.225	2.405	1.194	1.211	44.692
B3-2J	0.965	1.236	2.399	1.252	1.147	44.200
Average	1.003	1.325	2.383	0.919	1.464	38.024
Standard Deviation	0.032	0.103	0.018	0.341	0.325	6.332

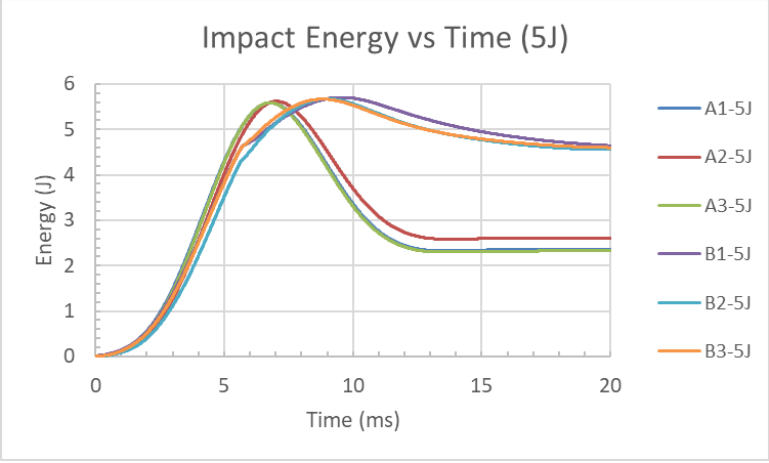

Figure 11. Energy vs time for 5J impact of transparent composites

Table 4. Impact results for 5J impact test on transparent composite

Sample	**Thickness (mm)**	**Max Force (kN)**	**Peak Energy (J)**	**Absorbed Energy (J)**	**Resting Energy (J)**	**Damage Area (mm^2)**
A1-5J	1.016	2.355	5.581	2.362	3.219	57.519
A2-5J	1.041	2.350	5.620	2.612	3.007	43.805
A3-5J	1.041	2.420	5.587	2.340	3.247	41.147
B1-5J	0.991	1.787	5.705	4.605	1.099	195.508
B2-5J	0.965	1.746	5.673	4.560	1.113	211.031
B3-5J	0.965	1.847	5.667	4.612	1.055	160.385
Average	1.003	2.084	5.639	3.515	2.123	118.232
Standard Deviation	0.032	0.293	0.046	1.081	1.037	72.489

17.86 ± 1.32 GPa with a tensile strength of 624.6 ± 32.8 MPa. The resulting flexural modulus was 19.69 ± 1.23 GPa, and the flexural strength was determined to be 155.7 ± 3.8 MPa. The impact behavior of the panels showed fair damage resistance with 0.919 ± 0.341 J of 2.383 ± 0.018 J impact energy absorbed and 3.515 ± 1.081 J of 5.639 ± 0.046 J of impact energy absorbed.

REFERENCES

1. F. Gibson, "A review of recent research on mechanics of multifunctional composite materials and structures," *Composite Structures,* Vol. 92, no. 12, pp. 2793-2810, 2010.

2. V. Menta, R. Vuppalapati, K. Chandrashekhara and T. Schuman, "Manufacturing of transparent composites using vacuum assisted resin transfer molding process," *Polymer and Polymer Composites,* Vol. 22, No. 9, pp. 843-849, 2014.

3. M. Grujicic, W. C. Bell, and B. Pandurangan, "Design and material selection guidelines and strategies for transparent armor systems," *Materials and Design,* Vol. 34, pp. 808-812, 2012.

4. P. G. Dehmer and M. A. Klusewitz, "High Performance Visors," Army Research Laboratory, Technical Report No. ARL-RP-45, 2002.

5. E. Strassburger, M. Hunzinger, J. W. McCauley, and P. Patel, "Experimental methods for characterization and evaluation of transparent armor materials," *Ceramic Engineering and Science Proceedings*, Vol. 31, No. 5, 2010.

6. X. Sun, C. Lai, T. Gorsich, and D. W. Templeton, "Optimizing Transparent Armor Design Subject To Projectile Impact Conditions," *Ceramic Engineering and Science Proceedings*, Vol. 29, No. 6, pp. 15-22, 2009.

7. J. Stenzler and N. Goulbourne, "Impact mechanics of transparent multi-layered polymer composites," Proceedings of the 2009 SEM 2009 Annual Conference & Exposition on Experimental & Applied Mechanics, Vol. 3, pp. 1963-1982, 2009.

8. A. Retegi, I. Algar, L. Martin, F. Altuna, P. Stefani, R. Zuluaga, P. Gañán, I. Mondragon, "Sustainable optically transparent composites based on epoxidized soy-bean oil (ESO) matrix and high contents of bacterial cellulose (BC)," *Cellulose*, Vol. 19, pp. 103-109, 2012.

9. K. Rai and D. Singh, "Impact resistance behavior of polymer nanocomposite transparent panels," *Journal of Composite Materials*, Vol. 43, No. 2, pp. 139-151, 2009.

10. D. Krug III, M. Ascuncion, V. Popova and R. Laine, "Transparent fiber glass reinforced composites," *Composites Science and Technology*, Vol. 77, pp. 95-100, 2013.

11. M. Velez, W. Braisted, G. Frank, D. Day and M. Mclaughlin, "Impact strength of optically transparent glass ribbon composites," *Journal of Composite Materials*, Vol. 46, No. 14, pp. 1677-1695, 2012.

12. ASTM International. D3039/D3039M-17 *Standard Test Method for Tensile Properties of Polymer Matrix Composite Materials*, West Conshohocken, PA, 2017. https://doi.org/10.1520/D3039_D3039M-17

13. ASTM International. *D7264 / D7264M-15, Standard Test Method for Flexural Properties of Polymer Matrix Composite Materials*, West Conshohocken, PA, 2015, https://doi.org/10.1520/D7264_D7264M-15

14. ASTM International. *D7136 / D7136M-15, Standard Test Method for Measuring the Damage Resistance of a Fiber-Reinforced Polymer Matrix Composite to a Drop-Weight Impact Event*, West Conshohocken, PA, 2015, https://doi.org/10.1520/D7136_D7136M-15

III. SOY-BASED POLYURETHANE COMPOSITES

Robert Meinders, Siva Dasari, Manoj Rangapuram, and K Chandrashekhara

Missouri University of Science and Technology
Department of Mechanical and Aerospace Engineering
Rolla, MO 65409

ABSTRACT

The development of new polymers can pave the way to sustainability in the future of composites. Soy-based polymer materials show the capability to replace petroleum polyols without significant material property loss. This paper will look at potential soy-based polymers to produce renewable polyurethane composites. HF-8450 and S300 soybean polyol are examined to produce polymers for continuous fiber reinforced composites. Formulations for thermoset polyurethane using soy-based polyol are developed for use in composites manufacturing. Continuous glass fiber-reinforced composite samples are manufactured using hand layup vacuum bagging process and the composite samples are characterized using flexure testing.

1. INTRODUCTION

Current dependence on petrochemical resources for the production of polyols poses future problems for polymers as these resources will eventually be depleted. Concerns over the production of greenhouse gasses tied to petroleum products also call for the development of renewable sourced materials [1-8]. Work is being performed to

allow for the use of renewable plant oils to replace traditional polyols and isocyanates with vegetable oil sourced materials [1-3, 9]. Polyurethanes manufactured using soybean, vegetable oil, and castor oils are showing promise as comparable replacements to petroleum polyols in rigid foams and plastics [4, 11-13]. Manufactured foams incorporating soy and vegetable oils are showing material properties that have some improvement at low percentage inclusions, and equivalent properties at higher percentage inclusions [5, 13]. Soy polyols are also showing promising results for improving polyurethane biodegradability and recyclability, both are concerns for the environmental impact of polymers [8, 9]. Soy polyols are also indicating potential improvements in biocompatible polymers, shape memory polymers, and self-healing polymer technology [2, 8, 14]. Polyols derived from soybean oil are also showing promise as a cheaper alternative to petroleum polyol and as a value added product for existing soybean oil processes [1, 11, 13].

Polyurethane polymers have a place in industry due to the wide range of material properties that can be achieved during manufacturing. Polyurethane can be developed into thermoplastic or thermoset materials by altering the functionality of the resin systems and controlling the polymer structures that are developed in the curing process [1, 5]. The addition of water and blowing agents can produce high quality foams that are rigid or flexible [4, 6, 9, 10]. Modifications can be made to polyol reactivity, functionality, molecular weight, and viscosity to tailor the polyurethane properties. Control over these chemical properties can be achieved based on the routes used to manufacture polyol from the base oils [1]. The production of polyurethane through isocyanate and polyol also

features low volatile organic compounds making it favorable for production processes [13].

Existing works focus on developing polyurethane foams that replace part of the petroleum polyol with renewable resourced polyols. This study examines the use of only soy oil polyol to develop non-foaming polyurethane composites. Different soy-based polyols are investigated for the development of a polyurethane for use in fiber reinforced composites. Composites are fabricated and tested to help promote the use soy-based polyol for increased sustainability of composite materials through the replacement of traditional petroleum polyols.

2. MATERIALS

This study uses soy polyols with Wanate PM-700, a commercially available isocyanate. The first selected polyol for the study was Feihang FH-8450. FH-8450 is a soy-based polyol that was chosen due to its high functionality. The material resin should be capable of producing thermoset composites with high networking for material strength and stiffness. Manufacturer specifications for FH-8450 are listed in Table 1 [15].

The other polyol in the study was Enviropol S300. Enviropol S300 is a soy-based triol with low viscosity for the production of polyurethane. The resin was selected for this study due to its current usage in a polymer blend to manufacture composite parts in Europe. This study removed the addition of petroleum polyols to evaluate the resin's use for renewable manufacturing. The properties of Enviropol S300 are listed in Table 2 [16].

Table 1. Properties of FH-8450

Hydroxyl Value	420+/-30 mg KOH/g
Acid Value	<0.5 mg KOH/g
Viscosity	3500+/-500 cps @25°C
Moisture	<0.1% w/w
Functionality (calculated)	8

Table 2. Properties of Enviropol S300

Hydroxyl Value	240-280 mg KOH/gm
Acid Value	<2.0 mg KOH/gm
Viscosity	320-350 mPas @25°C
Moisture	0.05% maximum
Functionality	3

3. MANUFACTURING

Soy polyurethane composites were fabricated using hand layup vacuum bagging process. Each soy polyol was combined with Wannate PM-700 isocyanate using a 1:1.05 polyol to isocyanate ratio. 28 cm x 28 cm panels were fabricated using four layers of E-glass fiber woven mat. The panels were fabricated on aluminum plates with Teflon release films. Polyurethane resin was infused into the fibers and the layup was sealed using a vacuum bag. The layup was cured at elevated temperature of 80 °C (175 °F) for 4 hours and cooled to room temperature.

4. EXPERIMENTATION

The flexural strength of the composite panels was evaluated using flexure testing as described in ASTM D 7246, “Standard Test Method for Flexural Properties of Polymer Matrix Composite Materials” [17]. Tests were conducted on a closed loop servo hydraulic Instron Model 5985 universal testing machine. The load was measured using a 10 kN load cell. Specimens were loaded in four-point bending with a recommended span to thickness ratio of 16:1. The rate of crosshead movement was set at 1.27 mm/min. The FH8450 composite panel with a measured thickness of 0.76 cm was cut into 15.24 cm x 2.03 cm samples. The S300 composite panel with a measured thickness of 0.33 cm was cut into 15.24 cm x 1.53 cm samples (Figure 1). Five specimens of each resin were tested and results are reported.

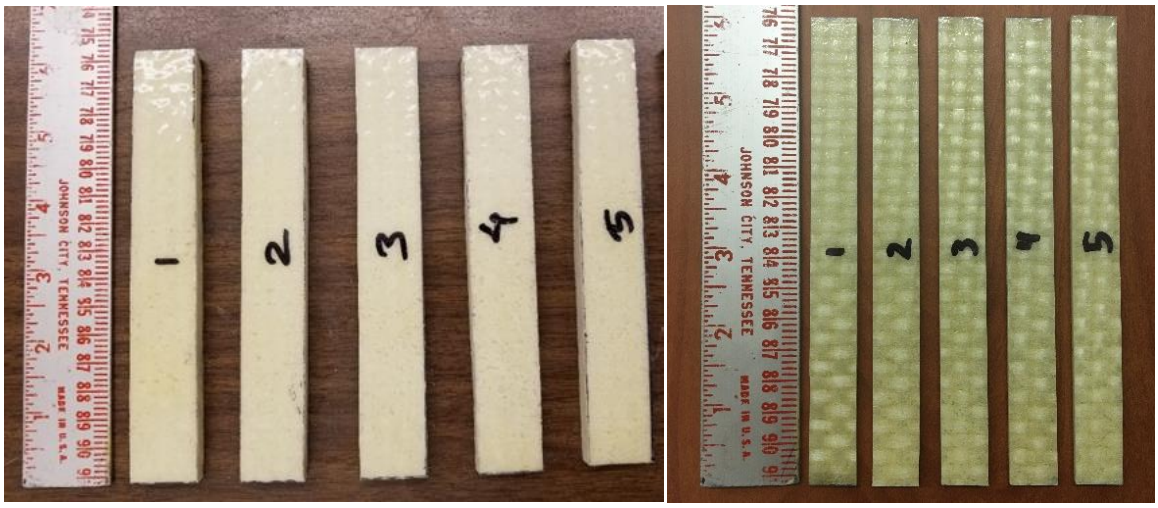

Figure 1. Test specimens (FH8450 left, S300 right)

5. RESULTS

The samples of FH-8450 composite were tested in four-point flexure using a span of 121 mm to achieve a 16:1 span to thickness ratio. The composite featured a linear response up to 0.007 flexural strain. Maximum stress developed at 0.017 mm/mm flexural strain and was followed by a large plastic deformation region (Figure 2). A flexural strength of 15.91 ± 1.3 MPa was calculated from the results which are compiled in Table 3. FH-8450 had a flexural chord modulus of elasticity of 1673 ± 214 MPa.

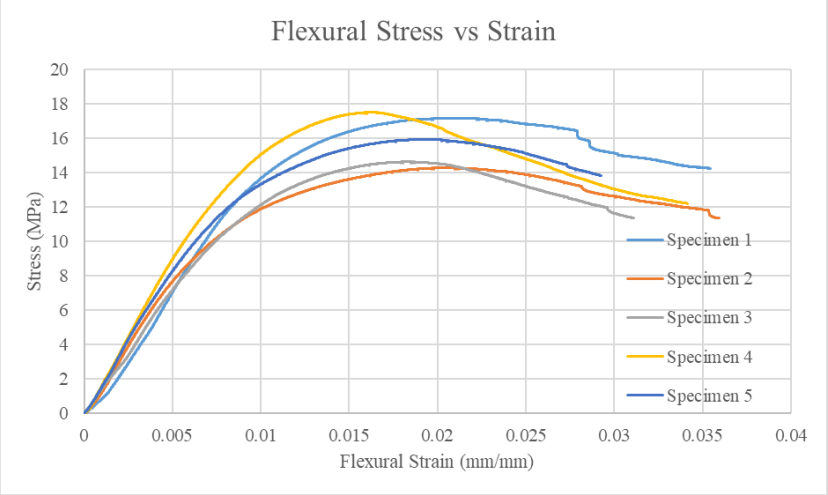

Figure 2. Stress vs deflection for Feihang FH-8450 polyol composite

The samples of S300 composite were tested in four-point flexure using a span of 53 mm to achieve the same 16:1 span to thickness ratio. The composite exhibited a linear elastic region up to 0.006 mm/mm flexural strain. Peak flexural stress occurred at 0.02 mm/mm flexural strain and was followed by a large plastic region of deformation (Figure 3). A flexural strength of 60.91 ± 4.60 MPa was calculated with results shown in Table 4.

Table 3. Results from flexural testing, FH-8450

Feihang FH-8450 resin	Flexural strength (MPa)
Sample 1	17.18
Sample 2	14.29
Sample 3	14.63
Sample 4	17.51
Sample 5	15.95
Average	15.91
Standard Deviation	1.30

It is of note that specimen 4 performed exceptionally well during the test and its omission leads to a lower average strength of 58.67 ± 1.11 MPa. Samples manufactured with S300polyol had a flexural chord modulus of elasticity of 7222 ± 1099 MPa or 6844 ± 893 MPa without including sample 4.

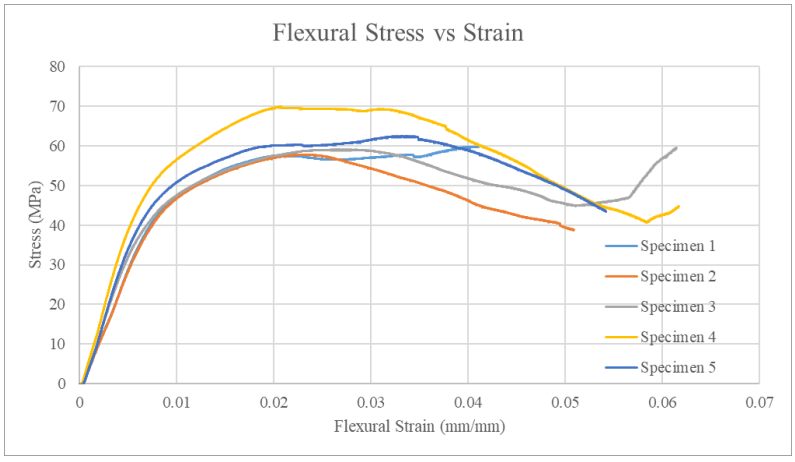

Figure 3. Stress vs deflection for Enviropol S300 polyol composite

Table 4. Results from flexural testing, S300

Enviropol S300 resin	Flexural strength (MPa)
Sample 1	57.53
Sample 2	57.77
Sample 3	59.06
Sample 4	69.90
Sample 5	60.31
Average	60.91
Standard Deviation	4.60

6. CONCLUSIONS

This study was able to produce composite polyurethane parts using only soy-based polyol and isocyanate. The FH-8450 samples produced below expectations for a high functionality polyol. This is thought to be caused by poor crosslinking and reduced reactivity of some of the hydroxyl groups. One of the concerns of using soy-based polyol is the reduced reactivity from the lack of primary hydroxyl groups compared to traditional petrol-based systems [Li]. Additional studies to increase the reactivity of FH-8450 will benefit the polyol to ensure the production of highly cross-linked polyurethanes. Additional reflections point to a degree of foaming in the FH-8450 composite which contributed to the increased thickness of the composite part and reduced part strength. Incorporating moisture scavengers will reduce this problem for production.

Enviropol S300 successfully generated a polyurethane composite with a measured flexural strength of 60.91 ± MPa.

This study was able to indicate that pure soy-based polyol composites are capable of being manufactured. Two different polyol resins were utilized to this effect and the composite properties were evaluated. The customization that is available in soy-based polyols should make the future production with renewable resources bright.

REFERENCES

1. Li, Y., Luo, X., and Hu, S., *Bio-Based Polyols and Polyurethanes*. Cham, Switzerland: Springer, 2015.

2. Miao, S., Wang, P., Su, Z., and Zhang, S., "Vegetable-oil-based Polymers as Future Polymeric Biomaterials," *Acta Biomaterialia,* Vol. 10, pp. 1692-1704, 2014.

3. Ourique, P., Krindges, I., Aguzzoli, C., Figueroa, C., Amalvy, J., Wanke, C., and Bianchi, O., " Synthesis, Properties, and Applications of Hybrid Polyurethane-urea Obtained from Air-oxidized Soybean Oil," *Progress in Organic Coatings,* Vol. 108, pp. 15-24, 2017.

4. Dhaliwal, G., Anandan, S., Chandrashekhara, K., Dudenhoeffer, N., and Nam, P. "Fabrication and Testing of Soy-Based Polyurethane Foam for Insulation and Structural Applications," *Journal of Polymers and the Environment,* Vol. 27, pp. 1897-1907, 2019.

5. Alagi, P., Choi, Y.J., and Hong, S.C., "Preparation of Vegetable Oil-based Polyols with Controlled Hydroxyl Functionalities for Thermoplastic Polyurethane," *European Polymer Journal,* Vol. 78, pp. 46-60, 2016.

6. Fang, Z., Qiu, C., Ji, D., Yang, Z., Zhu, N., Meng, J., Hu, X., and Guo, K., "Development of High-Performance Biodegradable Rigid Polyurethane Foams Using Full Modified Soy-Based Polyols," *Journal of Agricultural and Food Chemistry,* Vol. 67, pp. 2220-2226, 2019.

7. Mizera, K., and Ryszkowska, J., "Polyurethane Elastomers from Polyols Based on Soybean Oil with a Different Molar Ratio," *Polymer Degradation and Stability,* Vol 132, pp. 21-31, 2016.

8. Zheng, K., Tian, Y., Fan, M., Zhang, J., Cheng, J., "Recyclable, Shape-memory, and Self-healing Soy oil-based Polyurethane Crosslinked by a Thermoreversible Diels-Alder Reaction," *Journal of Applied Polymer Science,* Vol. 135, Issue 13, 46049, 2018.

9. Luo, X., Xiao, Y., Wu, Q., and Zeng, J., "Development of High-Performance Biodegradable rigid Polyurethane Foams Using all Bioresourced-based Polyols: Lignin and Soy Oil-derived Polyols," *International Journal of Biological Macromolecules,* Vol. 115, pp. 786-791, 2018.

10. Fan, H., Tekeei, A., Suppes, G., Hsieh, F., "Rigid Polyurethane Foams Made from High Viscosity Soy-Polyols," *Journal of Applied Polymer Science,* pp. 1623-1629, 2013.

11. Husic, S., Javni, I., and Petrovic, Z.S., "Thermal and Mechanical Properties of Glass Reinforced Soy-based Polyurethane Composites," *Composites Science and Technology,* Vol. 65, pp. 19-25, 2005.

12. Latere Dwan'isa, J., Mohanty, A., Misra, M., Drzal, L., and Kazemizadeh, M., "Biobased Polyurethane and its Composite with Glass Fiber," *Journal of Materials Science,* Vol. 39, Issue 6, pp. 2081-2087, 2004.

13. Vuppalapati, R., Menta, V., Chandrashekhara, K., and Schuman, T., "Manufacturing and Impact Characterization of Soy-Based Polyurethane Pultruded Composites," *Polymer Composites,* Vol. 35, Issue 6, pp. 1070-1077, 2014.

14. Petrovic, Z., Milic, J., Zhang, F., and Ilavsky, J., "Fast-responding Bio-based Shape Memory Thermoplastic Polyurethanes," *Polymer,* Vol. 121, pp. 26-37, 2017.

15. *Technical Data Sheet FH-8450.* Zhangjiagang Feihang Technologies, http://www.zjgfhkj.com, 2017.

16. *Enviropol S300 Technical Data,* Enviropol, www.enviropol.net.

17. ASTM International. *D7264/D7264M-15 Standard Test Method for Flexural Properties of Polymer Matrix Composite Materials*. West Conshohocken, PA, 2015. Web. 4 Dec 2019. <https://doi-org.libproxy.mst.edu/10.1520/D7264_D7264M-15>

SECTION

2. CONCLUSIONS AND RECOMMENDATIONS

2.1. CONCLUSIONS

The first study defined the material properties and responses during the layup and forming process to improve process performance and reduce defects and other manufacturing errors. Material characterization required to generate simulations of the prepreg forming process was performed. Material properties such as in-plane shear, fabric stiffness, and prepreg tack were experimentally measured for an 8-harness prepreg. Simulations of the material were used to determine the prepreg's reaction to compressive loading. Forming simulations of the prepreg were also performed to evaluate the feasibility of the simulation and check the proposed tooling for regions of wrinkling and defect formation.

The second study synthesized an epoxy resin system of Epon 826 and Epalloy 5200, with the cure hardener HHPA that was tailored to match the refractive index of an S-glass woven fabric upon cure. Epoxy resin was infused into a continuous fiber S-glass mat to produce transparent composite panels. The panels were inspected for visual transparency and tested for tensile, flexural, and impact properties. The resulting tensile modulus was 17.86 ± 1.32 GPa with a tensile strength of 624.6 ± 32.8 MPa. The resulting flexural modulus was 19.69 ± 1.23 GPa, and the flexural strength determined to be 155.7 ± 3.8 MPa. The impact behavior of the panels showed fair damage resistance with 0.919

± 0.341 J of 2.383 ± 0.018 J impact energy absorbed and 3.515 ± 1.081 J of 5.639 ± 0.046 J of impact energy absorbed.

The last study was able to produce composite polyurethane parts using only soy-based polyol and isocyanate. Feiheng FH-8450 polyol was employed to manufacture continuous glass fiber reinforced polyurethane composites. The material exhibited a flexural strength of 15.31 ± 1.30 MPa. Enviropol S300 was also used to successfully generate a soy-based polyurethane composite. The panel manufactured had a measured flexural strength of 60.91 ± 4.60 MPa. The two different polyol resins were utilized by this study and showed the feasibility of non-foaming soy-based polyurethane composites.

2.2. RECOMMENDATIONS

The works presented can be extended for future research. Additional studies on the forming of prepreg materials can be performed to examine how fiber weave and resin properties interact to predict the reaction of untested prepregs. Future work focusing on simulating thick laminate interactions and stacking effects within manufactured parts will prove invaluable to industry. Developing thick laminates using transparent composites and subjecting them to ballistics testing is the next leap forwards to producing lightweight transparent armors. Determining an effective lamination stacking sequence and comparing the properties to current technology is necessary for future ventures. The soy-based polyurethane composites are pushing the boundary towards renewable materials in the future. Experiments with additional polymers and developing a deeper understanding of the characteristics of soy-based polyols will encourage growth of renewable resources in the industry.

VITA

Robert Raymond Meinders was born in Bellevue, Nebraska. He received a Bachelor of Science from Missouri University of Science and Technology in both Aerospace and Mechanical Engineering in 2013. He then proceeded to earn his Master of Science in Aerospace Engineering from Missouri University of Science and Technology in 2015. He worked as both Graduate Research Assistant and Graduate Teaching Assistant throughout his graduate career at Missouri S&T. He received his Ph.D. in Aerospace Engineering from Missouri University of Science and Technology in August 2020.